"Railplug Ignition System for Enhanced Engine Performance and Reduced Maintenance"

Semi-Annual Technical Progress Report

Third 6 Months: October 1, 2002 - March 31, 2003

Ron Matthews, PI, Prof. of Mech. Engineering

29 September 03

DE-FG26-01NT41334

The University of Texas
1 Longhorn Station, C2200
Austin, TX 78712

DISCLAIMER

ABSTRACT

During the first 18 months of this project, four experimental subtasks were to have begun but only one of these was to have been completed. Additionally, five modeling subtasks were scheduled to begin, four of which were to have been completed. We are on schedule for all but one of these subtasks.

All four experimental tasks are progressing on schedule. Initial durability tests were completed. The conclusions drawn from this first round of durability tests are being used to design the next set of tests. Initial baseline engine data were acquired and showed that the engine selected for this task behaves as hoped. However, the dyno controller is inadequate. The engine will be moved to another dyno during the near future.

The modeling tasks are also progressing well. A model for the dynamic response of the ignition circuit was developed and validated. Two technical papers resulting from this model were submitted for publication. Development of a model for the railplug ignition process was begun but was not scheduled for completion. Progress on this task consisted of two subtasks. First, a railplug circuit model was also developed and validated. Second, a model was developed for the physics that govern railplug performance. This initial model incorporated only the effects of the Lorentz force on arc movement. From this model, it is concluded that thermal expansion is important to the performance of railplugs. Thermal expansion, and other physical effects, will be added to the model in the near future.

We delayed the development of a 3D model for the ignition process, until near the end of the project because of the computational time requirements. We can learn most of the important lessons from the 2D model. Delay of this subtask will not affect the timely completion of the project.

TABLE OF CONTENTS

LIST OF FIGURE CAPIONS

LIST OF TABLES

1. INTRODUCTION

The US Department of Energy established the Advanced Natural Gas Reciprocating Engine (ANGRE) program to improve large-bore stationary natural gas engines. The goals of the ANGRE program are to increase fuel efficiency to 50%, decrease emissions of the oxides of nitrogen (NOx) by a factor of 10, and decrease maintenance costs by 10%. Achievement of the efficiency and NOx goals of the program will require use of higher compression ratios and/or higher boost pressures and leaner air/fuel ratios. Both factors increase the demands upon the ignition system, whereas the ignition systems currently in use – for the present gas densities at ignition and mixture strengths – often fail to meet customer expectations for performance and durability. The ignition systems currently in use are derived from automotive applications and are not designed or optimized for the higher load, leaner conditions of large natural gas engines. There is, therefore, an acute need for a more robust ignition system for big natural gas engines offering longer igniter life and better ignition characteristics.

Via the ANGRE program, DOE funded a project at The University of Texas (UT) that consists of two simultaneous tasks. The experimental task is the development of a railplug and driver-electronics system designed around the unique requirements of stationary natural gas engines. Two sequential numerical tasks are also included in this project. First, we are expanding our prior model of spark ignition from a 2D transient simulation to a 3D transient version, incorporating flame chemistry for methane/air mixtures (the typical natural gas is more than 90% methane), and including the dynamics of the electronics circuit. This model will be useful as a new design tool for conventional spark plugs, optimizing the driver-electronics for spark plugs, and understanding ignition system dynamics and demands not only for current large bore natural gas engines, but also for future engines with higher boost pressures and air/fuel ratios. The second numerical task combines the improved spark plug model with a railplug model, to serve as an optimization design tool for development of railplugs for large bore natural gas engines.

The tasks and timelines that were incorporated in the proposal for this project are provided in Figure 1. The vertical dash-dot line highlights the first 18 months of the project. The beginning of each task is an open circle and the end is a filled circle. Vertical arrows show subtasks that feed into other subtasks. Lines that are linked (bold) feed each other throughout the duration of both. Four subtasks from the initial year were extended (Subtasks 1.1, 2.1.a, b, and c). Here, it should be noted that Subtask 1.1 is shown to be continuing even though we generated new railplug designs on schedule, because we will continue to improve the designs as we learn more throughout the course of the project. Two additional subtasks began at the end of the first year (Subtasks 1.5 and 2.2), neither of which was to have been completed at the end of the initial 18 months. Additionally, two subtasks that began at the end of the first 6 months are continuing through the end of the project. Progress on each of the tasks is discussed in Sect. 3.

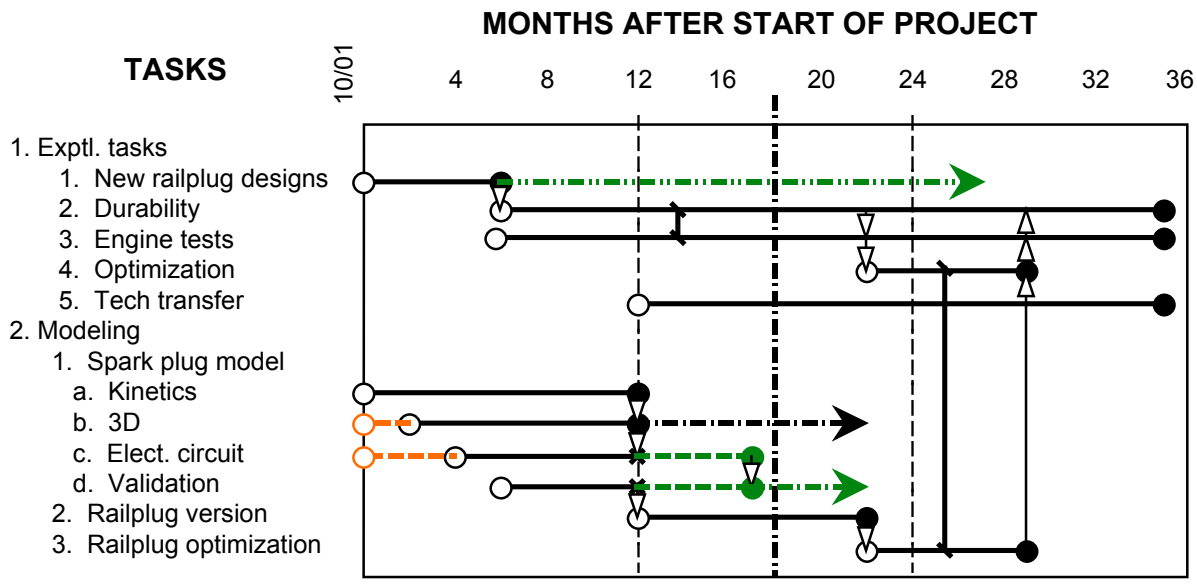

Figure 1. Tasks and timelines. The vertical dash-dot line highlights the first 18 months of the project.

2. EXECUTIVE SUMMARY

During the first 18 months of this project, four experimental subtasks were to have begun but only one of these was to have been completed. Additionally, five modeling subtasks were scheduled to begin, four of which were to have been completed. We are on schedule for all but one of these subtasks. Each of the tasks are discussed below.

Experimental Task 1.1, development of new railplug designs, was completed on schedule, but we will generate additional railplug designs as we learn more throughout the course of this project.

Experimental Task 1.2, durability testing was begun but was not scheduled for completion during the first 18 months. We fabricated a number of parallel railplugs and tested their durability using a Design of Experiments approach. From the durability experiments, it is concluded that the rail separation should be as small as practical and that three interactions are important: voltage and rail separation, capacitance and rail separation, and voltage and capacitance (energy). Additional parameters to be examined in the next set of durability experiments are rail length, void space, inductance, and electrode diameter.

Experimental Task 1.3, setup of the test engine, was completed. From the baseline engine experiments, it is concluded that the engine selected is intolerant of dilution, as expected. This will allow for easy determination of improvements. However, it is also concluded that the dyno controller is inadequate. The engine will be moved to another dyno during the near future.

Experimental Task 1.5, tech transfer, was begun by submitting two technical papers for publication.

Subtask 2.1.a, development of appropriate chemical kinetics mechanisms for the ignition process, was completed during the first year of the project. A simplified plasma kinetics mechanism was developed and tested against a detailed model. The agreement was quite good. A simplified kinetics mechanism for flame propagation was also developed and validated via comparisons against an elementary kinetics mechanism. Again, the agreement was quite good.

We delayed Subtask 2.1.b, development of a 3D model for the ignition process, until near the end of the project because of the computational time requirements. We can learn most of the important lessons from the 2D model. Delay of this subtask will not affect the timely completion of the project.

Subtasks 2.1.c and 2.1.d, development and validation, respectively, of a model for the dynamic response of the ignition circuit, were both completed. Specifically, a model for the dynamic response of the circuit for an inductive ignition system was developed and validated. The conclusion drawn from exercising this model is that only three circuit parameters – all of which involve the coil - have a significant effect on the energy deposition for an inductive ignition system. Increasing the turns ratio, increasing the core inductance, and decreasing the primary resistance all increase the energy deposition significantly. Decreasing the secondary resistance and the resistance of the high tension cable both increase the energy deposition, but with a weaker effect. The other circuit parameters, such as inductances and capacitances of the spark plug and spark plug wire, do not significantly affect the energy deposition for an inductive ignition system. Additional validations of this model are planned, including breakdown, arc, and higher gas densities. Also, a model for a CD ignition circuit is planned for development and validation. .

Task 2.2, development of a model for the railplug ignition process was begun but was not scheduled for completion. Progress on this task consisted of two elements. First, a railplug

circuit model was also developed and validated. From the railplug circuit model, it is concluded that 1) the resistor in parallel with capacitor C1 should be as large as possible, 2) the combination of capacitance C1 and charging voltage should be no larger than required to assure ignition, and 3) an inductor should be used to shape the current profile. However, the tradeoff between inductance and current must also be considered; as the inductance increases, the peak current and rate of current rise decrease. Also, the peak current decreases as the charging voltage decreases. The peak current and rate of current rise are important because they affect how rapidly the arc moves away from its position at breakdown. Second, a model was developed for the physics that govern railplug performance. This initial model incorporated only the effects of the Lorentz force on arc movement. From this model, it is concluded that thermal expansion is important to the performance of railplugs. Thermal expansion, and other physical effects, will be added to the model in the near future.

3. EXPERIMENTAL AND NUMERICAL TASKS

Progress on each of the experimental and numerical tasks that were scheduled for the third 6 months of this project is discussed in the following two subsections.

3.A. Experimental Tasks

The experimental tasks scheduled for the third 6 months of the project were to: 1) continue durability tests and 2) begin engine tests.

The initial durability tests were focussed upon parallel railplugs. The geometric variables for parallel railplugs are illustrated in Figure 2. The values used for the railplugs that were fabricated for the initial durability tests are provided in Table 1. The durability tests consisted of firing these railplugs to failure at atmospheric pressure. The results are discussed in Section 4.

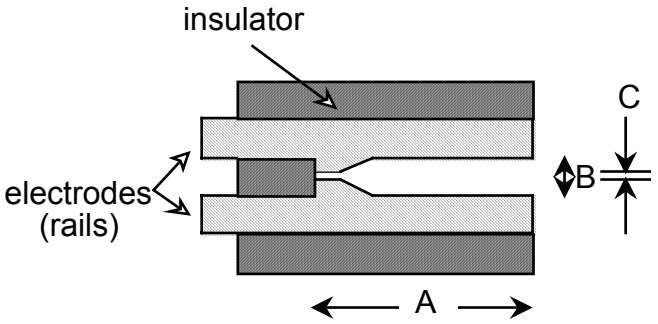

Figure 2. Parallel railplug, illustrating the dimensions that were varied for the initial designs.

Table 1. Parallel Railplug Designs that were Fabricated for Initial Durability Testing

	rail separation (mm/in)	rail length (mm/in)
min	0.508/0.020	2.0/0.079
	0.762/0.030	4.0/0.157
	1.016/0.040	6.0/0.236
	1.270/0.050	8.0/0.315
max	1.524/0.060	10.0/0.394

The second experimental task was to complete the setup of an engine for railplug performance and durability testing and to begin these tests. The only task remaining at the end of the first year before data could be acquired was installation of cylinder pressure data acquisition and analysis hardware. We are using a DSP Redhat cylinder pressure analysis system. This system is specially designed for high-speed engine data acquisition and analysis. This system was installed and calibrated during the third 6 month period. Initial baseline data were also acquired. These results are discussed in Section 4.

3.B. Numerical Tasks

The numerical tasks were to complete and validate a model for the ignition circuit and to begin generating a model for the railplug ignition process.

The circuit model was completed and validated. Two technical papers were generated from these tasks. The results are summarized in Section 4. A dashed arrow is shown for the validation subtask (2.1.d) in Table 1 because we plan to perform additional validation experiments.

Development of a model for the railplug ignition process (Task 2.2) was begun during the third 6 months. This model includes three components: an appropriate ignition circuit model, an appropriate description of the relevant physics, and a chemical kinetics submodel for both the plasma and flame propagation. The circuit model discussed in the previous paragraph was modified to make predictions for the unusual circuit that drives railplugs, as discussed in Section 4. The kinetics model developed during the first year is appropriate for railplugs, thus satisfying the third requirement for the railplug model. Thus, the only remaining issue is a numerical description of the relevant physics. This is challenging because the phenomena are complicated. First, a shock wave is generated during breakdown. For conventional spark plugs, this shock wave propagates into the combustion chamber and dissipates, without any significant effects. Breakdown occurs within the railplug, as illustrated in Figure 3 for a coaxial railplug. As also shown in Figure 3, there is a void space upstream of the initiation gap. When the shock wave is generated, it propagates both downstream (where is dissipates without significant effect) and also upstream. The upstream shock will heat the gases in the void space, reflect, heat the gases in the void space more, and the resulting thermal expansion will help to propel the already ignited mixture (upstream from the initiation gap out of the railplug muzzle. Additionally, the mixture in the void space may include fresh fuel/air mixture, depending upon the compression ratio and the volume ratio of the muzzle to void space. If so, combustion of the mixture in the void space will add to the thermal expansion. Finally, there is the issue of the Lorentz force, which accelerates the electrons in the plasma. This requires knowledge of the location and concentration of the electrons. Because electrons are not important to energy release within the plasma, they are not included in the kinetics scheme developed for this project. These issues add to the usual concerns, such as heat loss to the electrodes. Progress in this modeling effort is discussed in Section 4.

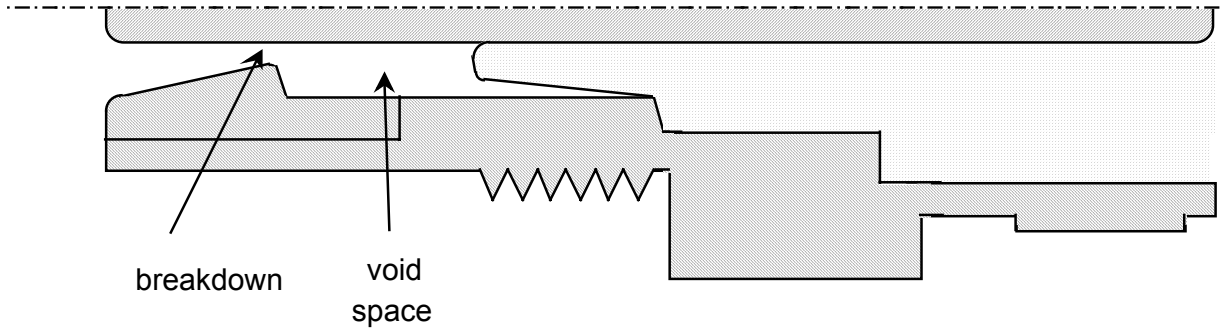

Figure 3. Schematic of a coaxial railplug, illustrating where breakdown occurs and the location of the void space.

Subtask 2.1.b is conversion of our 2-dimensional spark ignition model into a 3D model. However, the 2D model consumes a lot of computational time, and the 3D version will require

much more. Thus, we have decided to delay the 3D model to near the end of the project, when we will then focus on a few specific conditions to simulate.

4. **RESULTS AND DISCUSSION**

4.A. Experimental Tasks

The experimental tasks scheduled for the third 6 months of the project were to: 1) continue durability tests and 2) begin engine tests.

A set of Taguchi experiments was performed for the initial durability tests of parallel railplugs. Four factors were chosen, two design elements (gap and length) and two driver-circuit parameters (voltage and capacitance). Five levels were chosen for each. The factors and levels are shown in Table 2. An orthogonal array of four factors with five levels consists of 5^4 elements. The Design of Experiments allows this parameter space to be explored using only 25 experiments, as also shown in Table 2. Durability experiments were conducted at 1 atm and 298 K. The firing rate was 18.5 shots/s (the equivalent of ~2100 rpm), the spark gap varied with the rail separation (because the gap is only important to assure that breakdown can occur), and the rail diameter was 2.54 mm.

The durability of these railplugs was not very good, as shown in Tale 2. This was due to a discontinuity in the muzzle that held the arc. Nevertheless, several conclusions can be drawn from the results of these experiments. First, the rail separation should be as small as practical (our model for railplug physics, discussed in the next subsection, confirms this conclusion). Also, three interactions are important: voltage and rail separation, capacitance and rail separation, and voltage and capacitance (i.e., stored energy). The voltage affects the current, which drives the arc movement, and strongly affects the stored energy ($1/2CV^2$). The capacitance affects the stored energy, but more weakly than the voltage, and also affects the pulse duration (see discussion of railplug circuit model in the following subsection). Additional parameters to be examined in the next set of durability experiments are rail length, void space, inductance, and electrode diameter. Thus, the six parameters to be examined in the next Design of Experiments will be voltage, energy, inductance, electrode diameter, void, and rail length.

Table 2. Design of Experiments Matrix and Results

	Factors				
No.	Separation (mm)	Length (mm)	Voltage (V)	Capacitance (uF)	Durability (hours)
1	0.508	2	110	22	6.65
2	0.508	4	120	33	12.00
3	0.508	6	130	47	3.50
4	0.508	8	140	66	4.00
5	0.508	10	150	100	0.67
6	0.762	6	110	33	9.00
7	0.762	8	120	47	14.00
8	0.762	10	130	66	2.70
9	0.762	2	140	100	0.25
10	0.762	4	150	22	2.50
11	1.016	10	110	47	2.70
12	1.016	2	120	66	3.10
13	1.016	4	130	100	0.15
14	1.016	6	140	22	6.00
15	1.016	8	150	33	3.80
16	1.270	4	110	66	0.85
17	1.270	6	120	100	0.25
18	1.270	8	130	22	3.20
19	1.270	10	140	33	29.00
20	1.270	2	150	47	0.50
21	1.524	8	110	100	1.40
22	1.524	10	120	22	6.15
23	1.524	2	130	33	0.40
24	1.524	4	140	47	1.83
25	1.524	6	150	66	1.00

After installing and calibrating the cylinder pressure analysis system, initial baseline data were acquired. These results are illustrated in Figure 4. This figure shows the effect of equivalence ratio on the combustion instability for the baseline ignition system. The engine was operating on natural gas at wide open throttle and 900 rpm and MBT timing for each mixture. An 18 mm spark plug was used with an inductive ignition system. As shown in his figure, this engine is not very tolerant of dilution. In fact, the main reason that we chose this engine for the experiments was that we anticipated that it would not be dilution-tolerant, to highlight effects of the ignition process. However, a problem became apparent while performing these baseline experiments. Specifically, it was difficult to hold the engine speed at the desired setting due to problems with the dyno control system. We plan to move the engine to a different dyno in the near future.

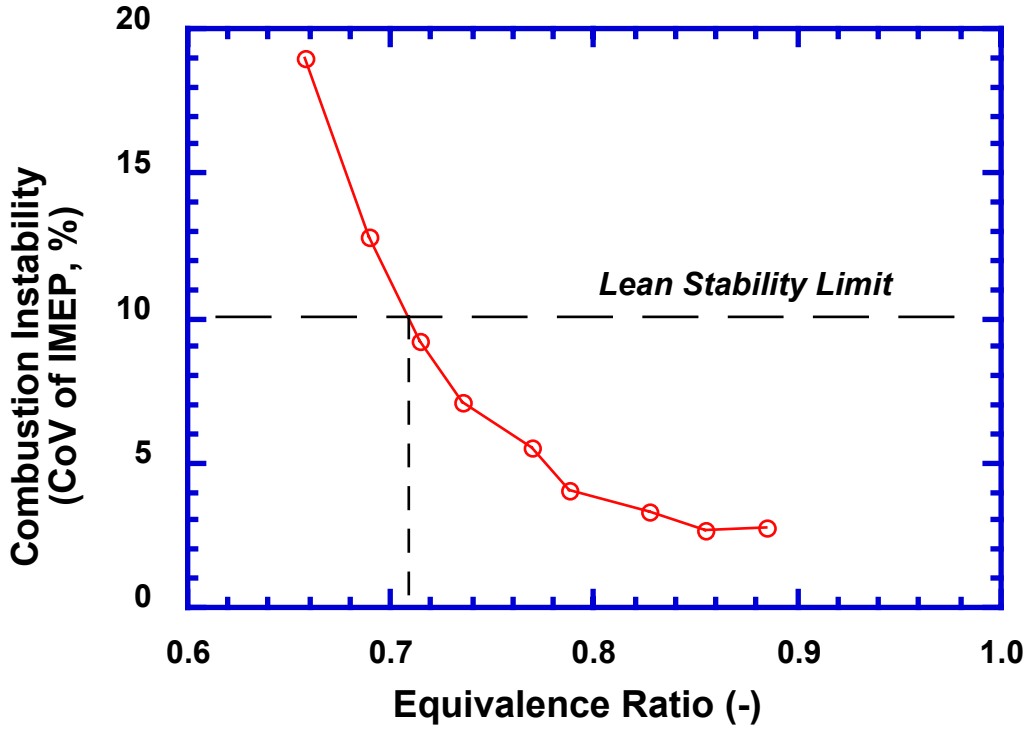

Figure 4. Initial baseline engine data.

4.B. Modeling Tasks

The numerical tasks during the third 6-month period were to complete and validate a model for the ignition circuits for both conventional ignition systems and railplugs, and to begin generating a model for the railplug ignition process. The results from each of these tasks are discussed in this subsection.

The spark can be divided into 4 basic phases: Pre-breakdown, Breakdown, Arc and Glow. The timing and duration of each phase is dictated by the characteristics of the ignition circuit (including the igniter). Pre-breakdown is the time period when the voltage of the coil is building until it is either large enough that a spark can jump the gap or, if the required breakdown voltage exceeds the capacity of the coil, a misfire will occur. Typically, this phase lasts for ~ 1 nanosecond. There is no energy deposition as there is no current flowing through the spark gap. As soon as enough ionizing electrons are produced to make the discharge self-sustaining, "breakdown" occurs. At breakdown, a highly conductive streamer (passage for electrons) is initiated, which leads to a sharp rise in current and sudden fall in voltage across the gap (Raether, 1964). This phase lasts for approximately 10 nanoseconds. There is very little energy deposition because of the short duration of this phase. Typically, between 0.3 and 1 mJ of energy, is deposited during breakdown. Breakdown may be perceived as a barrier that needs to be crossed to obtain a spark. Once breakdown occurs, the next phase, arc, begins. Arc is caused by the thermionic emission of electrons from the cathode surface (Loeb, 1939). The voltage drops rapidly to a low value (of around 50 V). The current starts to fall and the voltage stays at a constant value until a threshold value of the current is reached. The cathode surface temperature rises to ~3000 K, which is above the melting temperature of the cathode material at typical pressures. For this reason, the majority of the cathode erosion takes place during the arc phase. The electrons emitted from these pools are required to sustain the arc. The arc phase typically

lasts for ~10 microseconds and energy deposition is of the order of 1 mJ. Glow is the final phase of the spark. During glow, the mechanism of the emission of electrons from the cathode surface changes. The glow phase begins when the dominance of the thermionic emission of electrons ends. The bombardment of positive ions on the electrode surface now becomes the dominant mechanism (Meek and Craggs, 1953). Since this mechanism has a very low efficiency, the current decays to a low value (less than 1 A). The voltage, on the other hand, rises to a higher value (around 500 V). The glow phase is thus characterized by low currents and high voltages. The glow phase lasts for about 3 ms. During this period, 30-100 mJ of energy is deposited, which is far more than for the other three phases. This is mainly due to the fact that the duration of glow is longer. The glow ends when the current in the gap decays to near zero. Each of these phases was modeled.

A circuit-solving software package, PSPICE, is the heart of our model. It automatically accounts for the dynamic response of all types of conventional electronic components, such as capacitors, resistors, and inductors. However, the spark gap is not a conventional electronic component. Thus, the focus of our effort was modeling the spark gap for each of the phases of ignition. Schroeder's inductive ignition circuit model (Schroeder, 2002) was downloaded from the internet and modified for the present study. Each modification is listed below.

1. The model was altered to match the experimental ignition set-up used for validation.
2. The breakdown voltage was modeled as a function of spark gap and pressure.
3. The voltage during arc was modeled as a function of spark gap.
4. The voltage during glow was modeled as a function of spark gap.
5. The current at which the arc-to-glow transition occurs was quantified.

The static breakdown voltage can be obtained from Paschen's Law, which defines the breakdown voltage for different gases as a function of gap, temperature, and pressure for quiescent conditions and clean electrodes. Paschen's Law applies when the product of pressure times spark gap is less than 13.33 bar-mm (Bazelyan and Raizer, 1998), which is sufficient for the time of ignition in most light-duty engines and is close to the appropriate conditions for boosted large bore natural gas engines. For air, the static breakdown voltage is:

$$V_{BD} = 24.22x + 6.08\sqrt{x} \quad [\text{kV}] \tag{1}$$

where

$$x = \frac{293}{T}\frac{P}{1.013}\frac{g}{10} \quad [-] \tag{2}$$

where T is in K, P is in bar, and the gap, g, is in mm. Although Paschen's Law does not strictly apply to breakdown for spark plugs in engines, it is sufficient for the present purpose, which is to model the ignition process. So little energy is deposited during breakdown that the model needs only what the actual breakdown process provides – a trigger allowing the circuit to provide arc and glow.

The arc voltage consists of 3 basic components, namely the cathode fall (15 V), the anode fall (25 V) and the positive column (10 V/mm). The cathode and anode falls are narrow regions near the electrodes, where a sharp drop in potential occurs. The cathode fall is required for sustaining numerous cathode hot spots. The arc voltage can be defined as (Maly, 1984):

$$V_{arc} = 40 + 10g \quad [\text{V}] \tag{3}$$

The effects of pressure, temperature, and composition are discussed after the glow voltage model is introduced.

The glow voltage consists of the same 3 elements as the arc voltage: a positive column plus cathode and anode falls. However, the cathode fall voltage is very high during glow.

$$V_{glow} = 425 + 100g \quad [V] \tag{4}$$

The equations for arc and glow voltage will be different for different gases. However, since the gas encountered in engines is predominantly air, these equations should be accurate for all in-cylinder gas mixtures. Equations 3 and 4 are valid for all practical gap lengths and pressures because the anode and cathode fall form a very small portion of the gap length. When the gap is altered, only the length of the positive column changes appreciably and the anode and cathode fall regions remain unaltered (von Engel, 1965). Also, the cathode and anode fall voltages are not significantly affected by pressure (Howatson, 1976). The voltage of the positive column is independent of temperature and is a weak function of pressure. Therefore, it is reasonable to assume that the arc and glow voltage relations hold for all temperatures, pressures and mixture compositions encountered inside an engine.

The arc-to-glow transition occurs at a definite value of spark gap current. Most investigators put this limit at 0.1 A (Maly, 1984) without physical justification. It has been assumed that by the time the current has dropped to 0.1 A, the thermionic electron emissions (which are characteristic of the arc phase) have ended. The mechanism of electron emission from the cathode changes to bombardment of the positive ions and the transition to the glow phase starts. However, there are some unanswered questions related to the transition. The current in the gap is due to electron emissions from the cathode. This electron emission is governed by two basic mechanisms: 1) thermionic emissions and 2) bombardment of positive ions on the cathode. The total current can be found as a function of temperature by equating the energy transfer to the cathode and the radiated heat loss (Loeb, 1939). Consequently, the total current i is:

$$i = \frac{f\sigma T_c^4}{V_c} \quad [A] \tag{5}$$

where f is the cathode area in m^2, σ is the Stefan Boltzmann constant [5.67E-8 $W\text{-}m^{-2}K^{-4}$], T_c is the cathode surface temperature in K, and V_C is the cathode fall voltage. The thermionic emissions are a surface phenomenon on the cathode and the thermionic current is given by the expression (Loeb, 1939):

$$i_t = fAT_c^2 \exp(-B / T_c) \quad [A] \tag{6}$$

were A and B are Richardson Constants (Sze, 1969). The Richardson Constant B is

$$B = q\phi / k \quad [K] \tag{7}$$

Where q is the charge on an electron [1.602E-19 A-s/electron], ϕ is the work function of the metal [eV], and k is Boltzmann's constant [1.380E-23 J/K]. The value of the constant B was easy to find as the work functions of most metals are readily available (e.g., Sze, 1969). For metals, Richardson Constant (A) can be found from:

$$A \approx A^* = \frac{4\pi q m k^2}{h^3} \tag{8a}$$

where m is the effective mass and h is Planck's constant (6.63E-34 J-s). The effective mass depends upon the direction of current travel for semiconductors but is essentially the mass of a free electron for metals (Sze, 1969). Thus, for metals:

$$A \approx 1.2 \cdot 10^6 \quad [A/(m^2\text{-}K^2)] \tag{8b}$$

This leaves the cathode temperature as an unknown in Equations 5 and 6. Taking the ratio of the total current to the thermionic current (i.e. dividing Equation 5 by Equation 6) yields:

$$i / i_t = \frac{\sigma T_c^2}{A V_c \exp(-B / T_c)} \quad [-] \tag{9}$$

The unknowns in Equation 9 are the current ratio and the cathode surface temperature. An experiment conducted by Druyvesteyen (1939) was used to find the current ratio. Thermionic current of 0.1 mA was observed with a cathode diameter of 1.8 mm at a temperature of 2000 K (± 50 K). The cathode material used by Druyvesteyen was tungsten. Using a work function for tungsten of 4.4 eV yields B = 51078 K. Then from Equation 6, A = 121 A/cm2-K2, which agrees closely with Equation 8b. Inserting all values into the right hand side of Equation 9 yields $i/i_T \sim 1500$. If it is assumed that the thermionic current is 1500 times smaller than the total current at the time of the arc-to-glow transition, Equation 9 can be used to determine the cathode surface temperature at the time of this transition. Equation 5 can then be solved for the current at the time of the arc-to-glow transition (given the cathode fall voltage of 15 V). This procedure yields a current at the time of arc-to-glow transition that depends upon the cathode material. As examples, for a 2.8 mm cathode (typical for light-duty spark plugs), the transition current for nickel (ϕ = 4.50 eV) is 0.41 A and for platinum (ϕ = 4.72 eV) it is 0.51 A. The corresponding cathode temperatures (2053 K and 2162 K, respectively) are higher than the melting points for these two materials (1728 K and 2045 K, respectively). This corresponds with the fact that electrode erosion occurs during the arc phase; during glow the surface temperature is too low to sustain a melted surface.

Initial model validation was performed using an inductive ignition set up with the specifications shown in Table 3. All experiments were performed in air at 1 bar and 298 K. Additional validations for other conditions are planned for the future. The gap voltage was measured using a Tektronix P6015 voltage probe. This probe has an attenuation of 100. This was tested with a standard high voltage supply. This probe was inserted (clipped on) at the point where the spark plug wire connects to the spark plug. It effectively measures the voltage of the gap. This probe has high resistance and low capacitance so that it does not interfere significantly with the measured values. However, the time response of the voltage probe was insufficient to capture breakdown or arc. Thus, the model has only been validated for the glow phase at this time. A new voltage probe, with an attenuation of 1000, has been ordered to allow more comprehensive validation. The current in the spark plug wire was measured using a Pierson coil ("current loop").

Table 3. Description of the Experimental Ignition Circuit.

Parameter	Value
Turns ratio of coil	104
Resistance of primary windings	1.43 ohms
Resistance of secondary windings	14,000 ohms
Leakage Inductance of the coil	0.36 mH
Core inductance	6 mH
Resistance of the spark plug wire	8,000 ohms
Inductance of the spark plug wire	250 μH
Inductance of the spark plug	10 nH
Capacitance of spark plug and probe	70 pF

Figure 5 is an example comparison between the predicted and measured voltage histories. Breakdown and arc are not obvious on this graph due to the scaling. The agreement is very good except that the duration of the simulated glow is slightly shorter than the experimental value. The turns ratio of the coil, the resistance of the primary windings, and the core resistance strongly affect the spark duration. However, the turns ratio and the primary resistance were accurately determined. Therefore, it appears that the discrepancy in the spark duration is because the value of the core inductance supplied by the manufacturer was not accurate. If the core inductance is changed from 6 mH, to 8 mH, the spark duration for all cases examined also agrees well.

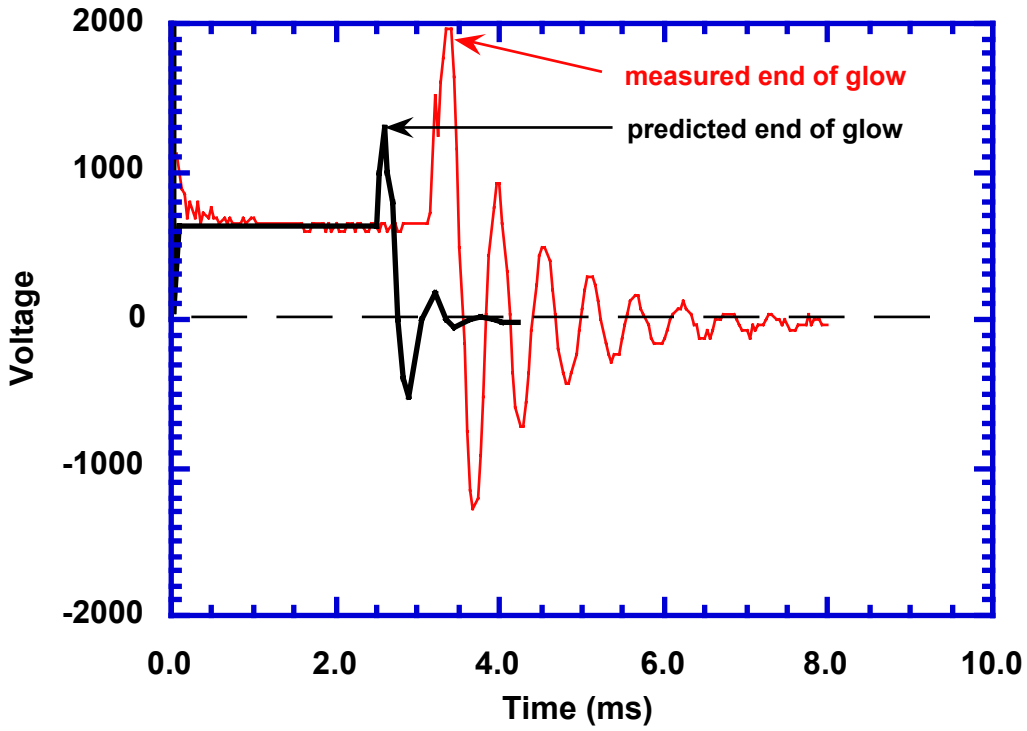

Figure 5. Comparison of predicted and measured voltage histories for a 2 mm spark gap at 1 bar, 298 K.

Table 4 shows the close agreement obtained between the model predictions and experimental data for the voltage during glow. Again, the agreement is quite good.

Table 4. Comparison Between the Experimental and Predicted Voltage during Glow.

Spark Gap (mm)	Predicted Voltage	Observed Voltage	Error (%)
0.7	495	500	1.00
1.0	525	540	2.78
1.5	575	620	7.26
2.0	625	620	0.81

3.0	725	740	2.03

Figure 6 is a comparison between the measured and predicted current histories. The model predicted that the current versus time profile is the same for all resistance values and gap lengths during the glow phase. This concurred with what was observed in the experiments. As shown in Figure 6, the current waveforms agree reasonably well given the significant noise in the signal.

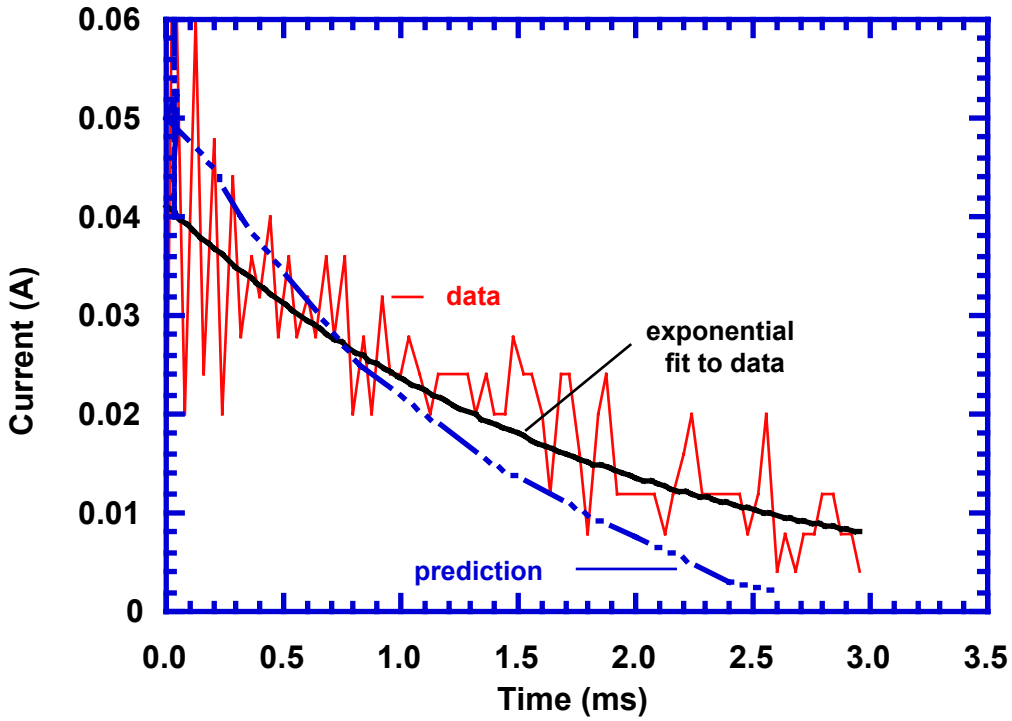

Figure 6. Comparison between experimental and predicted current histories.

The model was exercised to examine the effects of various circuit parameters on the ignition circuit dynamics for an inductive ignition system. Energy deposition during the glow phase dominates energy deposition for an inductive ignition system. Recall that the model has been validated for glow. We plan to perform similar simulations for a capacitive discharge ignition system in the near future once we perform validations for the arc phase. The conclusions drawn regarding energy deposition during the glow phase are summarized in Table 5. The other circuit parameters, such as inductances and capacitances of the spark plug and spark plug wire, do not significantly affect the energy deposition for an inductive ignition system. A paper has been submitted covering the circuit model for an inductive ignition system (Bhat et al., 2003a).

Table 5. Effects of Circuit Parameters for an Inductive Ignition System on Energy Deposition

Parameter (increasing)	Energy Deposited	Time to Deposit Energy	Extent of Impact
Turns ratio	increases	increases	significant
Primary resistance	decreases	decreases	significant
Core inductance	increases	increases	significant
Secondary resistance	decreases	decreases	weak
Spark plug wire resistance	decreases	decreases	weak

The railplug circuit model is a simple extension to the model for an inductive ignition system. As shown in Figure 7, the driver electronics for a railplug consists of an inductive ignition system – to provide breakdown – and a "follow-on circuit" that dumps its energy once a path is established by breakdown. The follow-on circuit provides the high current that is necessary to generate a Lorentz force to move the arc down the railplug muzzle. The primary components of the follow-on circuit are a capacitor (C2) that can be charged to an arbitrary voltage, and an inductor (L1). Both the capacitor and the inductor can be used to shape the current profile. The follow-on circuit also includes a diode (D1) to prevent the breakdown current from flowing into the follow-on circuit, a resistor (R2) in parallel with the diode to discharge any remaining voltage after the arc has ceased, and a blocking capacitor (C1) to prevent the current from the follow-on circuit from flowing backward through the coil.

The railplug circuit model was validated by performing experiments with a parallel railplug at 1 atm and 298 K. The spark gap at the breech was 1 mm and the parallel rails were 2 mm apart and 10 mm long. The current flowing through the railplug was used for validating the model. Experimental data was taken with various follow-on capacitors and a range of initial charge on the capacitor. Figure 8 illustrates the comparisons between the predictions and the experiments. Table 6 compares the peak current measured during the experiments and the model predictions. The agreement is quite good.

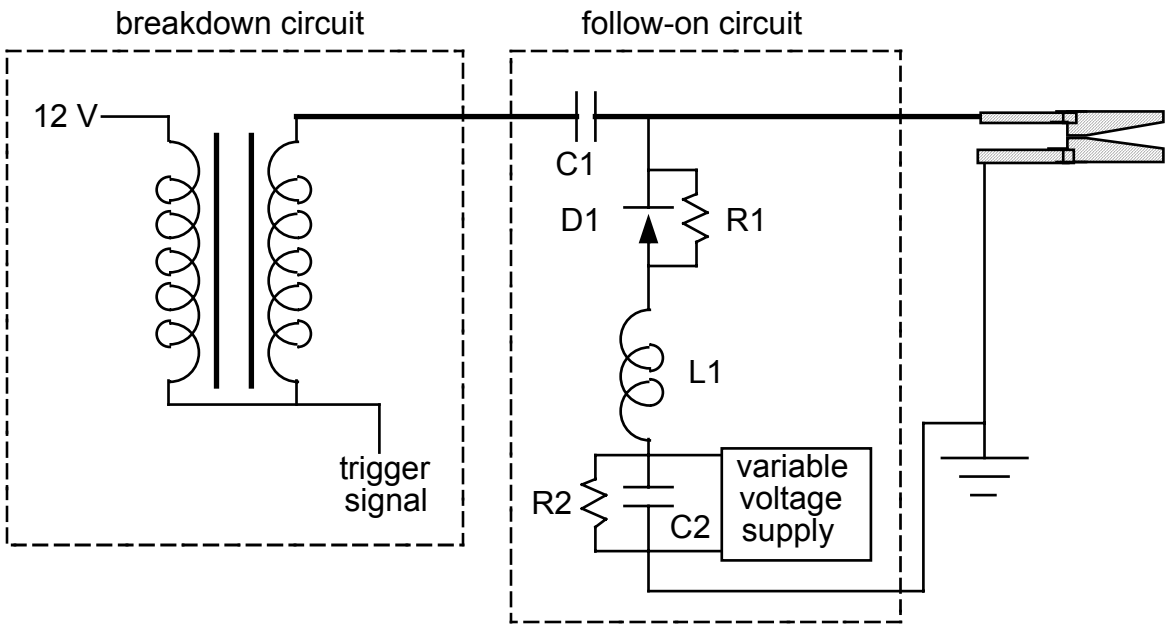

Figure 7. Schematic of railplug driver circuit.

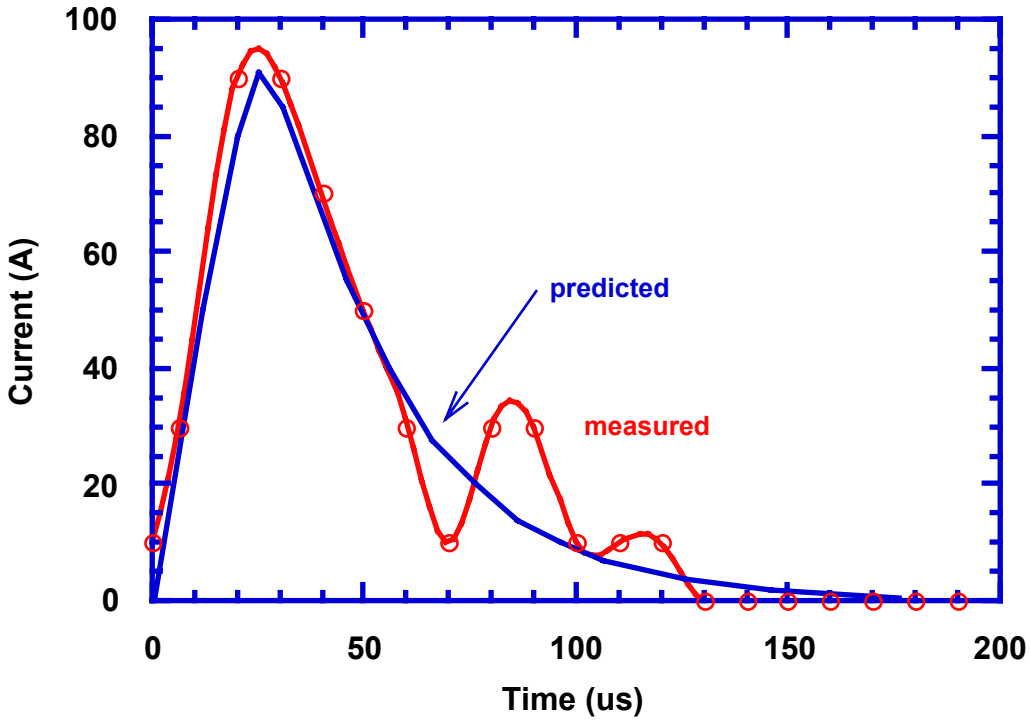

Figure 8. Comparison between model predictions and experimental current profile for a capacitance of 33 μF charged to 100 V.

Table 6. Comparison Between Measured and Predicted Peak Currents.

Capacitance	Charging Voltage	Predicted	Measured	Error

(mF)	(V)	Peak Current (A)	Peak Current (A)	(%)	
33	100			91	92
1.1					
47	100			79	75
5.3					
130	100			87	93
6.5					
330	115			103	102
0.9					
330	95	90		90	0.0

After validating the model for the railplug circuit, the model was used to explore the effects of the various circuit parameters. Figure 9 illustrates the effects of the capacitance (C2). For a fixed charge of 100 V, increasing the capacitance increases both the stored energy and the energy delivered to the railplug gap, and also increases the duration of the arc. As another example, Figure 10 shows that the inductance (L1) can be used to stretch out the current duration without having a significant effect on the delivered energy. Table 7 shows the overall results of this exploration. Circuit parameters not noted in this table did not have a significant effect on either the energy delivered or its duration. It is concluded that 1) the resistor in parallel with capacitor C1 should be as large as possible, 2) the combination of capacitance C1 and charging voltage should be no larger than required to assure ignition, and 3) inductor L1 should be used to shape the current profile. A paper has been submitted covering the railplug ignition circuit model (Bhat et al., 2003b). However, the tradeoff between inductance and peak current must also be considered, as illustrated in Figure 11. Also, the peak current decreases as the charging voltage decreases, as shown in Figure 12. The peak current and rate of current rise are important because they affect how rapidly the arc moves away from its position at breakdown.

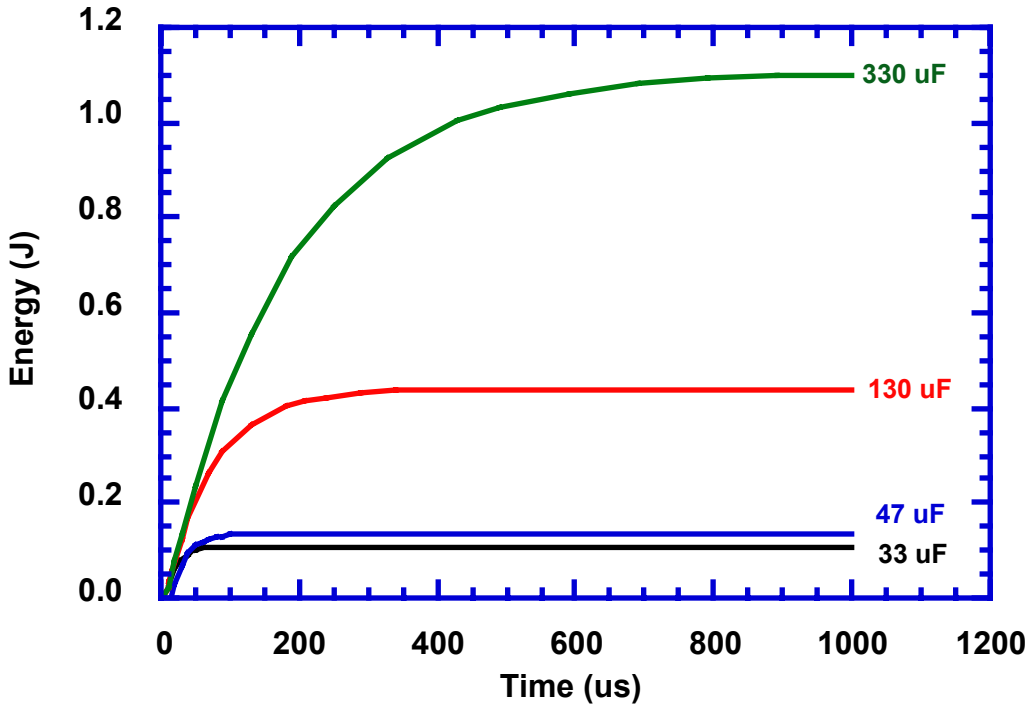

Figure 9. Effect of follow-on circuit capacitance on energy delivery for an initial charge of 100 V.

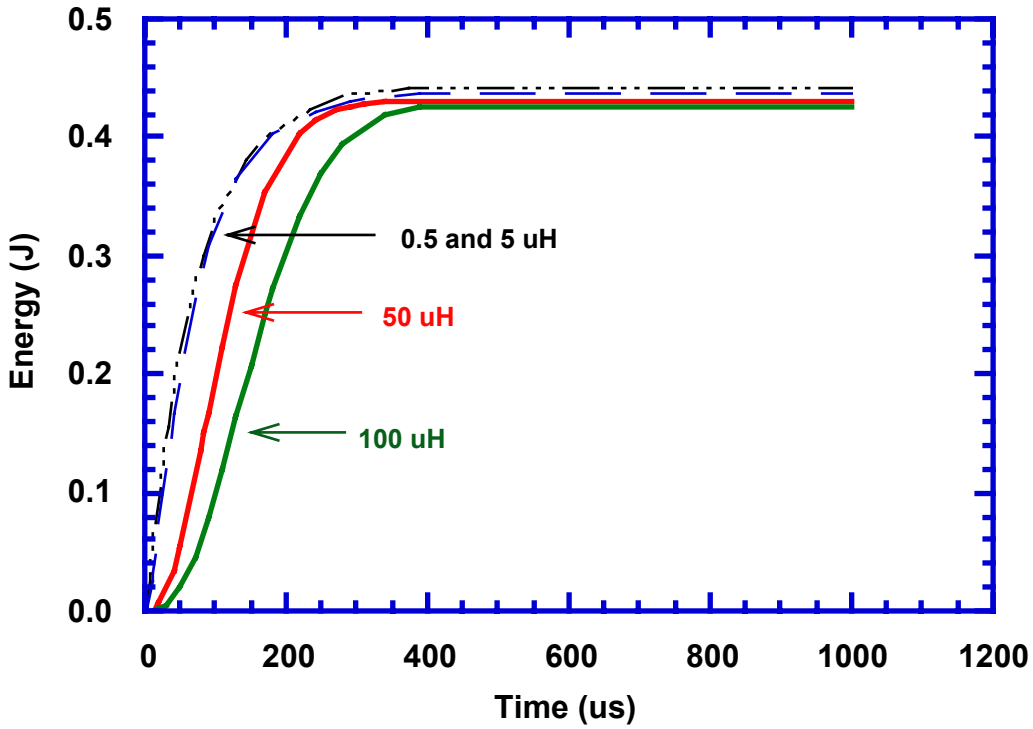

Figure 10. Effect of follow-on circuit inductance on energy delivery for a capacitance of 130 µF and an initial charge of 100 V.

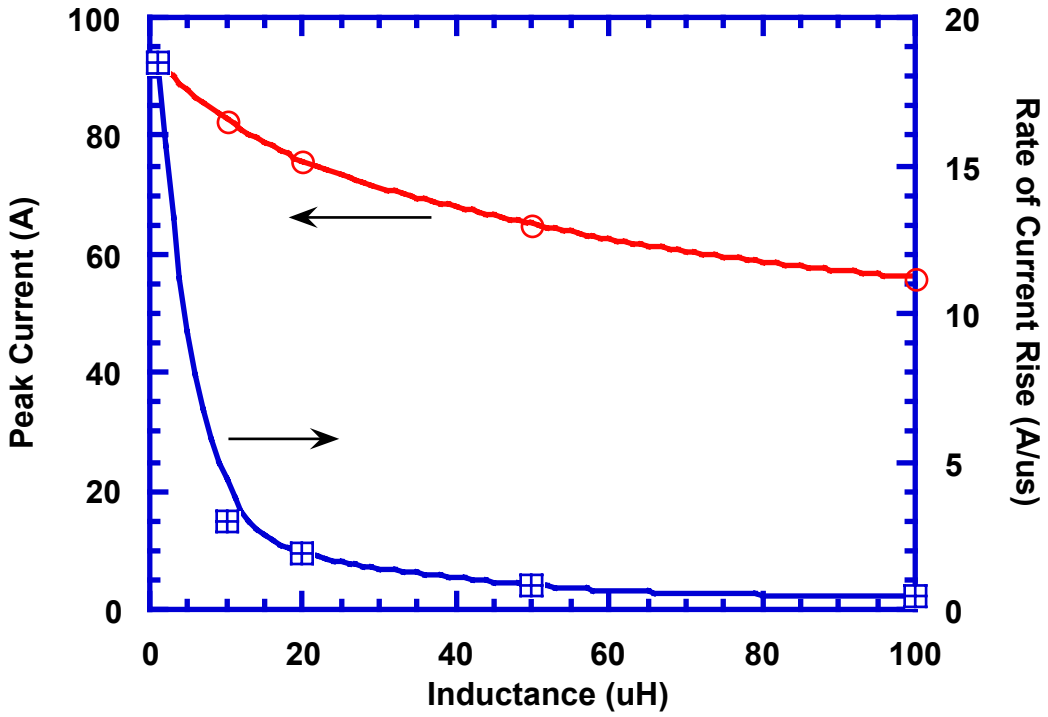

Figure 11. Increasing the inductance stretches out the current delivery but also decreases the peak current and the rate of current rise.

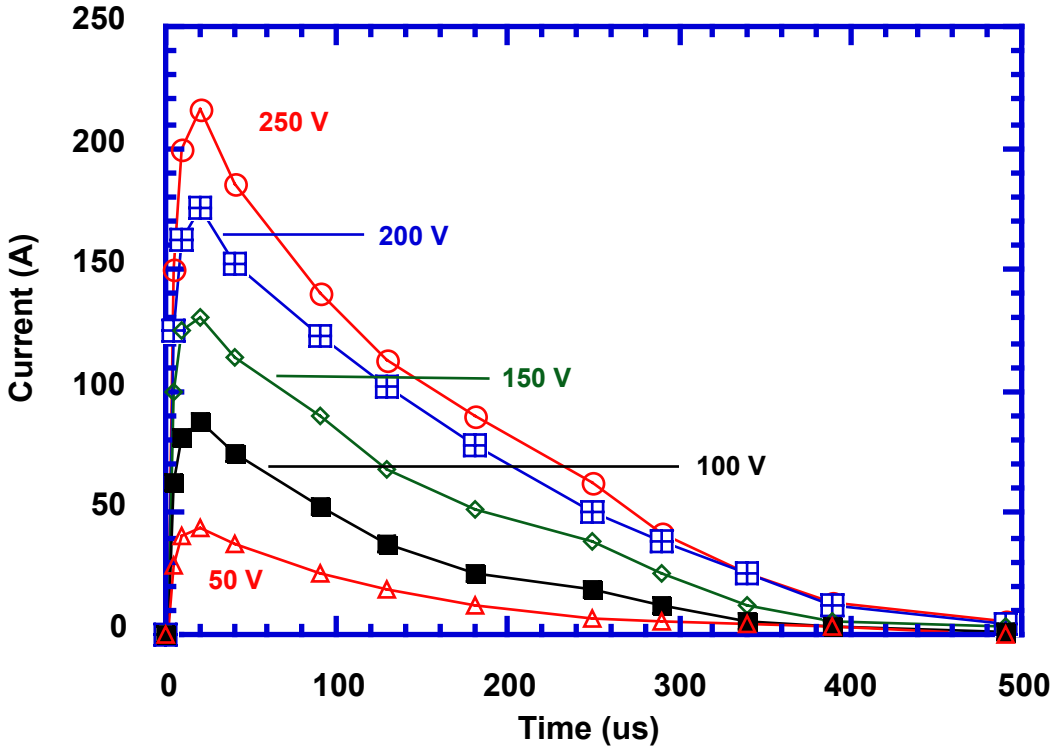

Figure 12. The charging voltage affects the peak current but not the rate of current rise.

Table 7. Effects of Circuit Parameters for Railplug Ignition System on Energy Deposition

Parameter (increasing)	Energy Deposited	Time to Deposit Energy	Impact on Energy	Impact on Duration
Capacitance C2	increases	increases	significant	significant
Charging voltage	increases	no effect	significant	no effect
Inductance L1	no effect	increases	weak	significant
Parallel resistance R2	increases	no effect	significant	no effect

Development of a multidimensional model for the railplug physics began by formulating the equations for arc movement generated only by the Lorentz force. A parallel railplug, for which experimental data for the arc movement was available, was simulated. The current supplied by the driver electronics is shown in Figure 13. The results are illustrated in Figures 14 and 15. The arc velocity and movement are greatest along the rail surfaces, because the electromagnetic field strength is highest here and decays toward the centerline. The arc accelerates as the current increases and decelerates after the current has peaked. By 190 μs, the arc velocity is approaching 100 m/s and the arc has moved almost 10 mm. However, the peak current used for these experiments and simulations may be higher than desirable for durability – one of the goals of the simulations is to provide a design tool for maximizing durability but with acceptable performance.

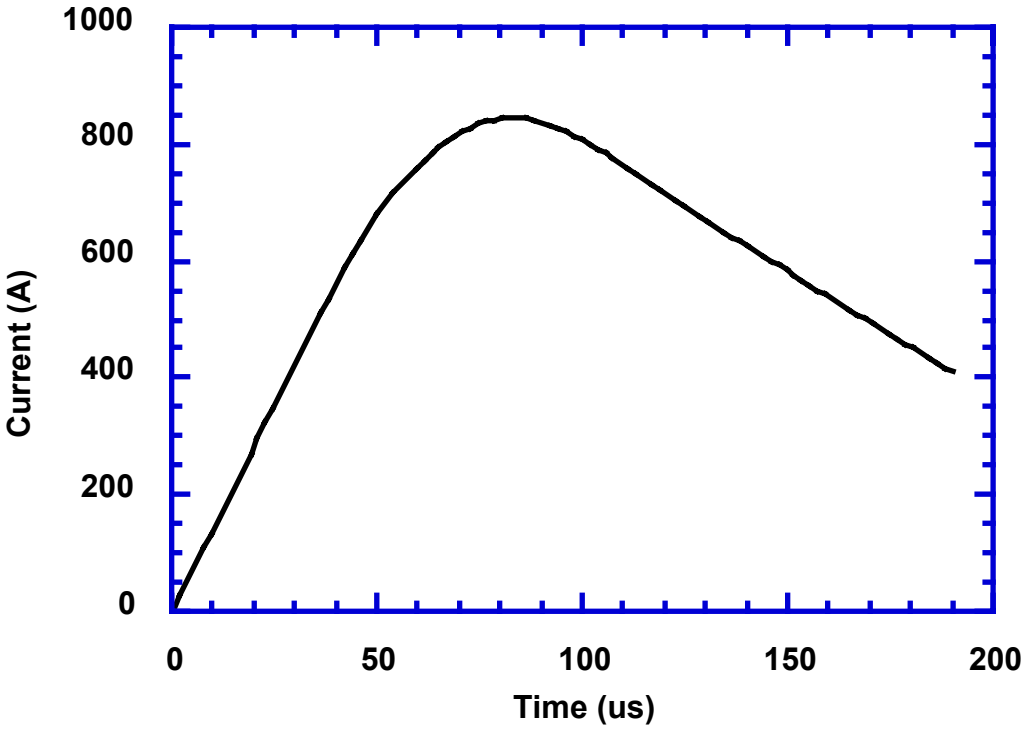

Figure 13. Current profile used for the simulations and associated experiments.

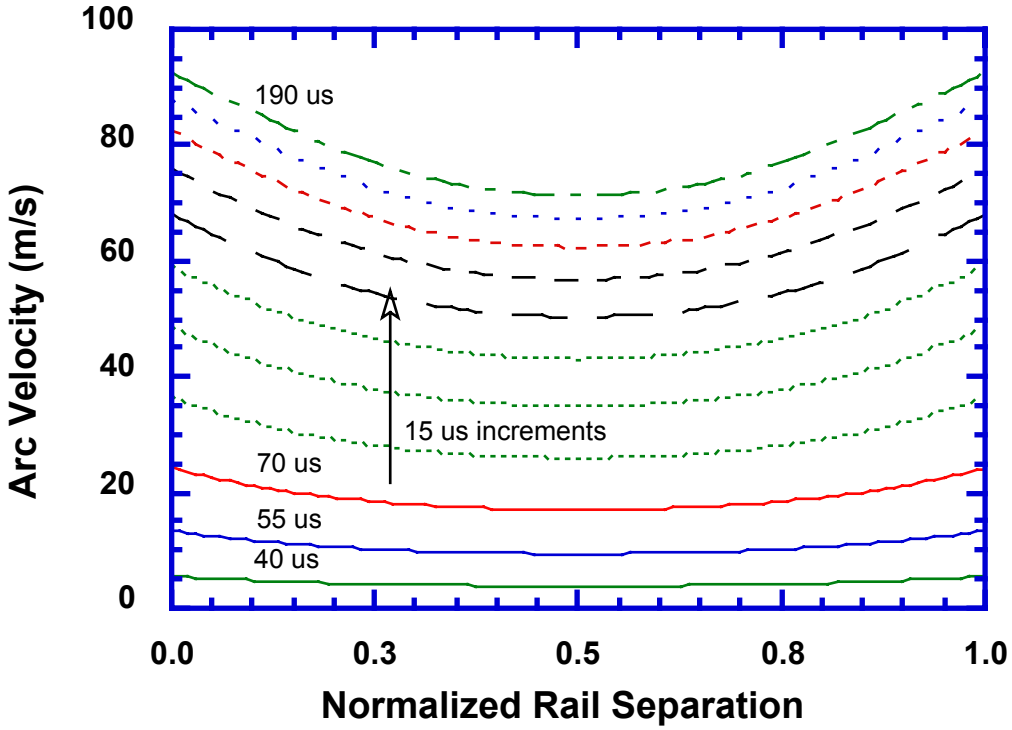

Figure 14. Arc velocities resulting solely from the Lorentz force for a parallel railplug.

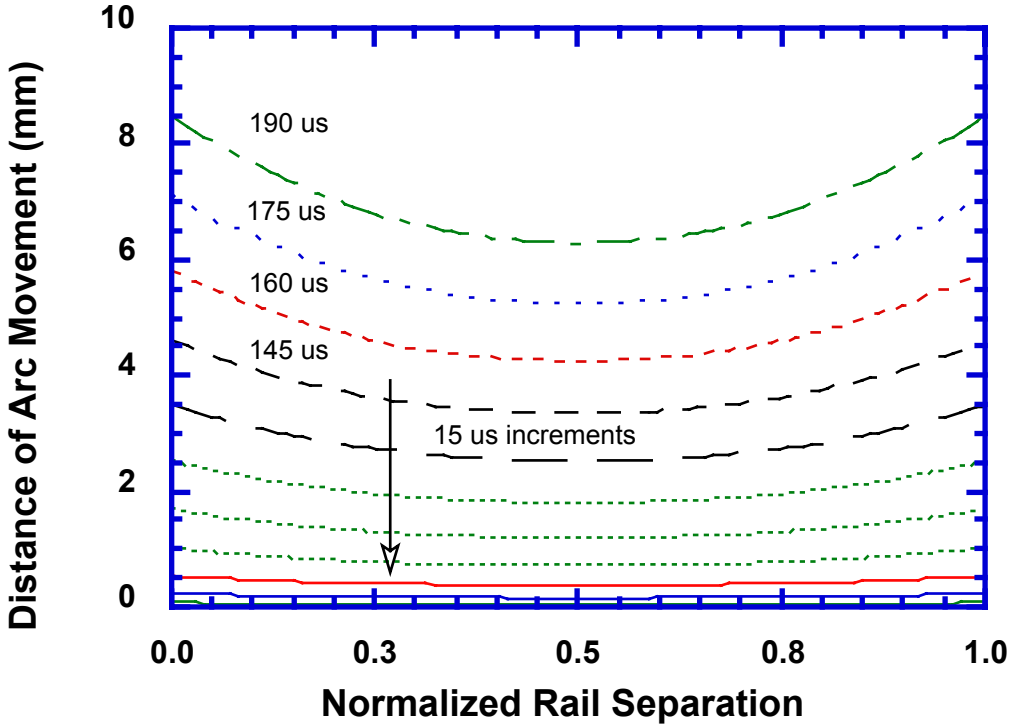

Figure 15. Arc motion resulting solely from the Lorentz force for a parallel railplug.

Figure 16 compares the model predictions with experimental data. The predicted arc velocity is much slower than measured. This indicates that thermal expansion is also important, even when the medium is only air, as it was for these experiments. Thus, the next task is to add thermal expansion into the model. Additionally, several assumptions were used to obtain the predictions discussed above, and these assumptions can be removed once the model is more complete.

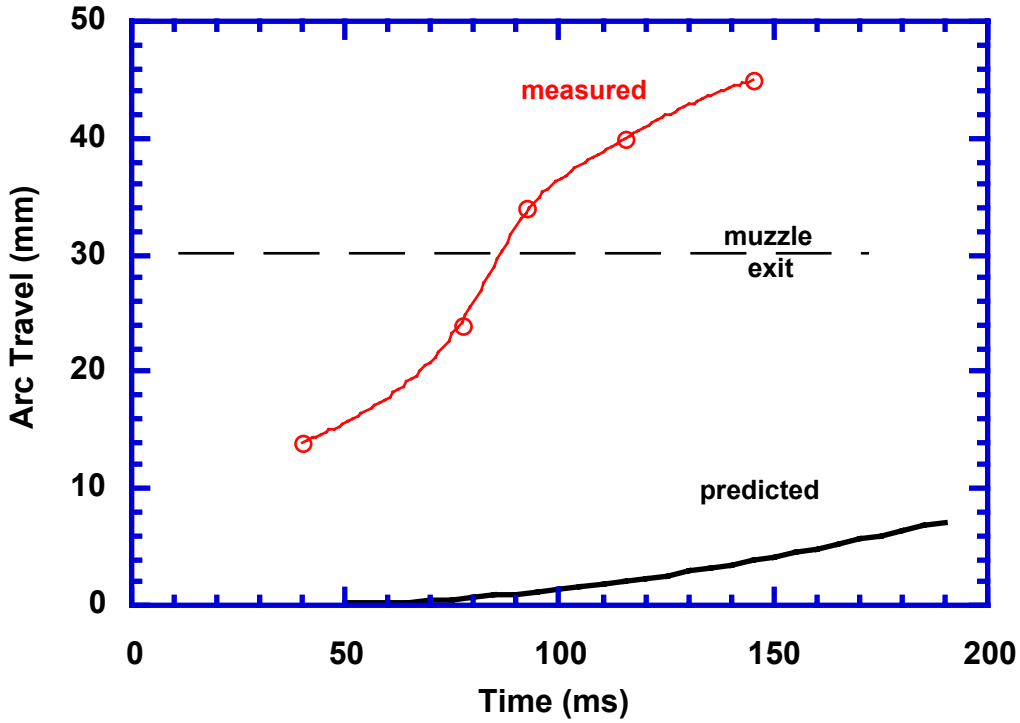

Figure 16. Comparison of predicted and measured arc motion for a parallel railplug.

5. CONCLUSIONS

The experimental tasks are on schedule. From the durability experiments, it is concluded that the rail separation should be as small as practical and that three interactions are important: voltage and rail separation, capacitance and rail separation, and voltage and capacitance (energy). Additional parameters to be examined in the next set of durability experiments are rail length, void space, inductance, and electrode diameter. From the baseline engine experiments, it is concluded that the engine selected is intolerant of dilution, as expected. This will allow for easy determination of improvements. However, it is also concluded that the dyno controller is inadequate. The engine will be moved to another dyno during the near future.

The modeling tasks are also progressing well. A model for the dynamic response of the circuit for an inductive ignition system was developed and validated. The conclusion drawn from exercising this model is that only three circuit parameters – all of which involve the coil - have a significant effect on the energy deposition for an inductive ignition system. Increasing the turns ratio, increasing the core inductance, and decreasing the primary resistance all increase the energy deposition significantly. Decreasing the secondary resistance and the resistance of the high tension cable both increase the energy deposition, but with a weaker effect. The other circuit parameters, such as inductances and capacitances of the spark plug and spark plug wire, do not significantly affect the energy deposition for an inductive ignition system. Additional validations of this model are planned, including breakdown, arc, and higher gas densities. Also, a model for a CD ignition circuit is planned for development and validation. . A railplug circuit model was also developed and validated. From the railplug circuit model, it is concluded that 1) the resistor in parallel with capacitor C1 should be as large as possible, 2) the combination of capacitance C1 and charging voltage should be no larger than required to assure ignition, and 3) inductor L1 should be used to shape the current profile. However, the tradeoff between inductance and current must also be considered; as the inductance increases, the peak current and rate of current rise decrease. Also, the peak current decreases as the charging voltage decreases. The peak current and rate of current rise are important because they affect how rapidly the arc moves away from its position at breakdown. The final model developed during this period was a model for railplug physics. This initial model incorporated only the effects of the Lorentz force on arc movement. From this model, it is concluded that thermal expansion is important to the performance of railplugs. Thermal expansion, and other physical effects, will be added to the model in the near future.

The combined results of our railplug physics model and the initial durability experiments dictate that the rail separation must be as small as possible. However, we need to assure that the spark jumps the gap near the breech (upstream) end. We must also avoid any discontinuities in the rail profile since these can hang the arc (preventing downstream movement of the arc). Thus, we have decided upon a slight taper to one electrode for the parallel design, or to the outer electrode for the coaxial design. For either design, this taper corresponds to a 5 degree angle between the rails, with the closest gap at the breech.

REFERENCES

Bazelyan, E.M., and Y.P. Raizer (1998), Spark Discharge, CRC Press, Boca Raton.

Bhat, S., O.A. Ezekoye, and R.D. Matthews (2003a), "Impact of ignition circuit characteristics on spark gap energy deposition", submitted to the *International Journal of Engine Research*.

Bhat, S., O.A. Ezekoye, and R.D. Matthews (2003b), "Impact of railplug circuit parameters on energy deposition and durability", accepted for the SAE Powertrain Conference, Pittsburgh, October.

Druyvesteyen, M.J. (1939), Z. Physics, 770, Vol. 111.

Howatson, A.M. (1976), An Introduction to Gas Discharges, Permagon Press, Oxford.

Loeb, L.B. (1939), Fundamental Processes of Electrical Discharge in Gases, John Wiley and Sons, New York.

Maly, R. (1984), "Spark ignition: its physics and effect on the internal combustion process", Chapter 3 in Fuel Economy of Road Vehicles Powered by Spark Ignition Engines, J.C. Hilliard and G.S.Springer (editors), Plenum Press, New York.

Meek, J.M., and J.D. Craggs (1953), Electrical Breakdown of Gases, Oxford at the Clarendon Press, Chapter 12.

Raether, H. (1964), Electron Avalanches and Breakdown in Gases, Butterworths, Washington.

Schroeder, C. (2002), www.beyond-designs.com/pspice_inductive.htm (accessed March 2002)

Sze, S.M. (1969), Physics of Semiconductor Devices, Chapter 5, John Wiley and Sons, New York.

von Engel, A. (1965), Ionized Gases, second edition, Oxford at the Clarendon Press.